

Broadband RF Energy-Harvesting Arrays

This article compares design methodology and scalability of narrowband and broadband rectenna arrays for RF energy harvesting.

By ERIC KWIATKOWSKI^{ID}, Member IEEE, JOSÉ ANTONIO ESTRADA^{ID}, Member IEEE, ANA LÓPEZ-YELA, Member IEEE, AND ZOYA POPOVIĆ^{ID}, Fellow IEEE

ABSTRACT | For RF energy harvesting, where the frequencies, power density, polarization, and direction of incident waves are unknown and variable, broadband rectenna arrays offer a simple scalable approach. In this article, we first compare the design methodology and scalability of narrowband and broadband arrays. An example 10-GHz narrowband rectifier array is presented to showcase the challenges involved in ultralow-power (down to $1 \text{ mW/m}^2 = 0.1 \text{ } \mu\text{W/cm}^2$) ground-based harvesting of narrowband satellite signals. The circularly polarized array consists of subarrays with RF power combining before rectification. This approach is then contrasted to harvesting over a wide RF bandwidth, through a comparison of several broadband arrays with rectifiers in each element. This includes a 2–5-GHz bow-tie screen-printed wearable rectenna array with an efficiency exceeding 30% above $50\text{-}\mu\text{W/cm}^2$ incident power density and a 2–18-GHz spiral array tested with powers down to $0.1 \text{ } \mu\text{W/cm}^2$. The two types of arrays are analyzed in the context of applications in a ground-based satellite transmitter with narrowband directional power receiver and in a broadband case with multiple widely spaced simultaneous signals.

KEYWORDS | Energy harvesting; multitone; power combining; rectenna array; rectifying circuit; Schottky; wearable; wireless power transfer (WPT).

I. INTRODUCTION

Wireless power transfer (WPT) using electromagnetic (EM) fields has a broad range of applications, from

delivering kilowatt power levels to electric vehicles from the road at kHz and low MHz frequencies, to enabling low-power sensors powered by ambient EM radiation in the microwave and millimeter-wave ranges. A comprehensive review and historical background of various applications and methods for WPT are given in, e.g., [1] and [2], while a unified design approach is given in [3], and an overview of a WPT international project is presented in [4].

Energy harvesting, sometimes referred to as scavenging, is a far-field type of WPT. It can be narrowband and directive when the source is known or broadband and nondirective when very low power densities are received from one or more known or unknown transmitters [5]. The energy is collected by antennas, coupled to low-power rectifiers and stored over an extended time period in a storage element [6]. This is practical for low duty cycle and low power consumption devices, such as unattended wireless sensors, e.g., [7] and [8].

Harvesting of different wireless transmitters is demonstrated in the literature, including mobile base stations around 2 GHz [9], [10], broadcast TV in the UHF range [11], Wi-Fi [12], ZigBee [13], multiple ISM bands [14], [15], satellite transmitters for monitoring of the satellite itself [16], and airplane altimeter sidelobes for structural health monitoring sensors [17]. Demonstrations of devices powered by RF harvesting include a quartz clock [18], wearable biological sensors [19], [20], and so on. The harvested energy is typically stored in a supercapacitor, e.g., [21], or solid-state battery [22].

For RF energy harvesting applications, where the frequencies, power density, polarization, and direction of incident waves are unknown and variable, broadband rectenna arrays offer a simple scalable approach, as illustrated in Fig. 1. Several modulated waves are incident on an array of size N that consists of M -element subarrays ($M \geq 1$) that combine the very low received RF power with minimal loss and deliver it to a rectifier. The rectified power is dc-combined and delivered to the application,

Manuscript received June 22, 2021; revised October 18, 2021; accepted November 23, 2021. Date of current version January 6, 2022. This work was supported in part by the Naval Research Laboratory through a contract with Envisioneering under Grant 19-02-0131-V101. The work of Zoya Popović was supported by Lockheed Martin through the Endowed Chair for RF Engineering and the Chair of Excellence, University Carlos III of Madrid, Spain. (Corresponding author: Zoya Popović.)

The authors are with the Department of Electrical, Computer and Energy Engineering, University of Colorado Boulder, Boulder, CO 80309 USA (e-mail: zoya@colorado.edu).

Digital Object Identifier 10.1109/JPROC.2021.3134658

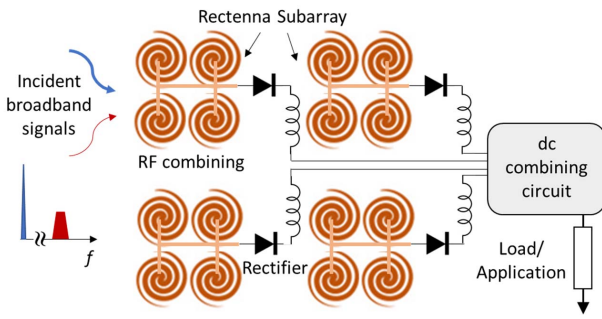


Fig. 1. Illustration of RF energy harvesting arrays that offer scalability in terms of the amount of harvested energy and a reconfigurable dc impedance. Several modulated waves are incident on a N -element array that consists of M -element subarrays ($N = M = 4$ in the figure) that combine the very low received RF power with minimal loss and deliver it to a rectifier. The rectified power is dc-combined and delivered to the application, e.g., a sensor.

e.g., to a sensor or to a battery, preferably through an efficient power-management circuit.

This article focuses on a discussion of the benefits of RF harvesting arrays and some design challenges. Section II presents a review of previous work in harvesting arrays with a summary of main parameters and design approaches as they apply to narrowband and broadband arrays. Section III showcases the general idea through an example of a specific narrowband rectenna array for ground-based ultralow-power-density ($0.1 \mu\text{W}/\text{cm}^2$) rectification of 10-GHz satellite transmitters. This known transmitter case is then contrasted with ambient harvesting from unknown wireless transmitters with broadband arrays. Two specific implementations are compared in Section IV: a dual-circularly polarized (CP) multioctave (2–18 GHz) array and a dual-linearly polarized 2–5-GHz wearable array. Section V presents analysis and measurements in an application context. First, the narrowband array is analyzed in a ground-based satellite transmitter harvesting application, followed by an analysis of multiple widely spaced simultaneous signals harvested by broadband arrays.

II. ARRAYS FOR RF HARVESTING

A number of narrowband arrays for energy harvesting have been demonstrated for communication-related applications, such as monitoring base-station activity in the LTE 1.96-GHz band [23], [24], for harvesting GSM-900 [25], GSM-1800 [26], UMTS-2100 [27], and 2.45- [28]–[30] and 5.8-GHz [31], [32] ISM bands. A narrowband 10-GHz array for harvesting satellite transmitter power is shown in [33]. Several authors have investigated dual-band arrays for harvesting multiple communication bands, e.g., arrays for 915 MHz/2.45 GHz [15], as well as 1.8/2.1 GHz [34], [35], are tested with incident power in individual or simultaneous bands. Two 6–15- [36] and

2–18-GHz arrays of left- and right-hand CP spirals for broadband harvesting of unknown sources are shown in [37]. Bow-tie dual-polarized arrays in the 2–5.8-GHz sub-6-GHz 5G band are shown in [38], and a wearable device around the same band is demonstrated in [39]. A lower frequency fractal dual-polarized broadband array covering GSM, UMTS, Wi-Fi, and LTE2600/4G bands (≈ 1.3 – 2.6 GHz) is shown in [40].

A summary of broadband arrays is given in Fig. 2, where the incident power density varies over several orders of magnitude, and the frequency range is from 900 MHz to 18 GHz, with the following conclusions.

- 1) Higher frequency arrays have lower efficiency, as expected due to the loss of standard Schottky diodes in the rectifier circuits, e.g., [33] compared to [34].
- 2) The efficiencies are greater at higher incident power levels, as expected for an exponential diode I – V curve.
- 3) The efficiencies are generally higher for narrowband arrays at comparable low incident power densities and at lower frequencies. Although some broadband arrays show peak efficiencies that are higher than in the narrowband case, e.g., [37] compared to [34], the efficiency is highly variable across the wide bandwidth.
- 4) The dual-band array [15] tested with simultaneous signals shows an improved efficiency. This also holds for simultaneously incident waves at two or more frequencies within the bandwidth of a broadband array (see Section V).

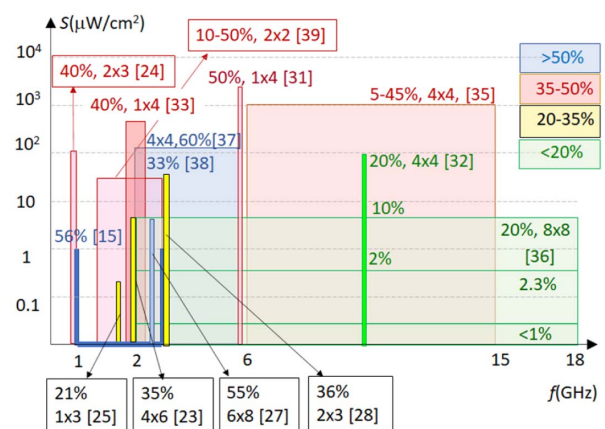


Fig. 2. Comparison of published arrays for RF harvesting applications as a function of frequency and incident power density. The efficiency ranges are color-coded, and the efficiency and number of array elements given for each reference. The dual-frequency array in [15] is tested with two simultaneous CW signals at 915 MHz and 2.45 GHz. (Note: the authors took the liberty to estimate some of the values since not all information is given in all papers.)

The remainder of this section discusses the main design steps and performance metrics for narrowband and broadband harvesting rectenna arrays.

A. Rectifier Impedance Matching

To achieve high conversion efficiency at low incident power densities, the rectifier nonlinear impedance should be matched to the antenna impedance with the lowest possible loss. In a narrow bandwidth, the source pull of the rectifier over a range of power levels and dc loads determines the target complex impedance range. The antenna or array is then codesigned to present this target impedance to the rectifier for the lowest possible loss, using one of the following approaches.

- 1) Direct complex conjugate matching between diode and antenna feed point. One example is an indented feed of a patch antenna with a complex impedance of $(30 - j240) \Omega$ at 4.3 GHz, which directly conjugately matches a rectifier impedance of $(38 + j252) \Omega$ at -15 -dBm input power for a $5\text{-k}\Omega$ dc load [17]. This network is implemented in microstrip on a Rogers 4350B substrate with a single Skyworks SMS7630-061 GaAs Schottky diode, and a Texas Instruments BQ25504 PMM chip is used to set the effective dc resistance seen by the rectifier to the optimum value and enable efficient capacitor charging at $0.65\text{-}\mu\text{W}/\text{cm}^2$ incident power density. Another example is in [29], where the diode impedance of $(26 - j29) \Omega$ at 2.45 GHz and -15 -dBm input power for a $5\text{-k}\Omega$ load is conjugately matched with a folded dipole and filter in the dc collection circuit. The rectenna is fabricated on a 2-mm-thick Plexiglas substrate with 95% optical transparency, making it appropriate for placement on, e.g., windows.
- 2) Rectifier and antenna impedance both matched to 50Ω . In this case, typically, only $|s_{11}|$ is presented, as in, e.g., [41], and implicitly requires matching circuits with additional loss. To reduce loss, the rectifier circuit can be designed to have an impedance closer to 50Ω .
- 3) Antenna impedance is designed to be complex, but the diode impedance cannot be reached directly. In this case, a complex prematch is performed on the antenna side, with a simple low-loss matching circuit between the antenna and rectifier. An example is shown in [10], where a patch feed point impedance of $(38 - j48) \Omega$ is matched with a simple cascaded transmission-line circuit to the desired $(137 + j149) \Omega$ of the rectifier.
- 4) Rectifiers fed by multipoint antennas, as in [42] and [43], where a tightly coupled n -element array is designed with $p < n$ feed to rectifiers. Tightly coupled arrays with a rectifier in each element, e.g., [38], [45], and [46], are versions of this approach. In these cases, there is no explicit matching circuit, and the broadband impedance of the tightly coupled

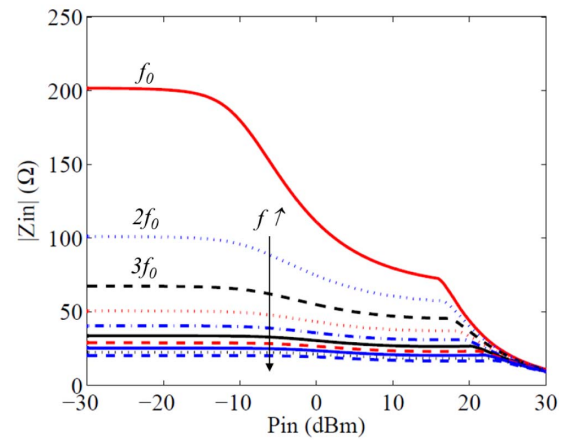


Fig. 3. Simulated magnitude of input impedance of Skyworks SMS7630-79 diode as a function of input power over a decade bandwidth for $f_0 = 2.45$ GHz.

array is matched over a part of the frequency range to the diode [37].

Fig. 3 shows a harmonic balance simulation of the magnitude of the input impedance of a shunt diode over a range of input powers and across a decade bandwidth. The impedance of this diode at the fundamental frequency of $f = 2.45$ GHz does not vary significantly for low power levels corresponding to harvesting, but it is clear that designing a rectenna for harvesting will force a degraded efficiency at higher power. In the broadband case, the impedance varies significantly over frequency at all power levels. In addition, there is a variation in optimal dc load, making it more difficult to design an antenna with a good match over all parameters. As a result, the efficiency of broadband arrays can vary significantly over frequency, e.g., in [40] from 10% to 50% over the 1.3–2.6-GHz band and 5%–45% in [36] in Fig. 2. In arrays that have over an octave of bandwidth, the elements are coupled at the lower frequencies, changing the impedance at each feed point. The Bode–Fano criterion dictates fundamental limitations of a broadband matching network, given for a single reactive element in Bode’s initial work [46] and extended to a more general two-port network by Fano [47]. The extension to limitations for diode mixer matching [48] shows that the principle is valid for networks such as a rectifying diode matched to an antenna.

B. RF and DC Power Combining

Harvesting arrays scale power as the number of elements increases, with a tradeoff in efficiency related to the size of the subarray in Fig. 1. In many harvesting arrays, each antenna element is loaded with a rectifier, e.g., [29], [47], and [51], and consequently, the rectifiers operate in the low-power and low-efficiency regime. RF combining at the input can be useful to boost the efficiency and is straightforward in the narrowband case

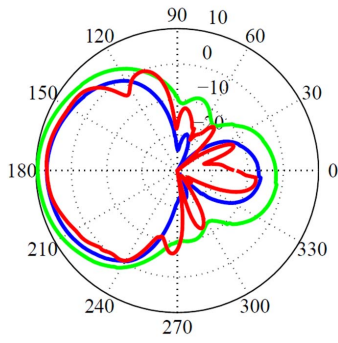


Fig. 4. Normalized measured 50- Ω -matched 1.96-GHz patch antenna pattern (green). Predicted dc power pattern for a power density of 200 $\mu\text{W}/\text{cm}^2$ (blue) from measured conversion efficiency as a function of input power from [23] and measured rectenna pattern at power density of 200 $\mu\text{W}/\text{cm}^2$ (red).

with corporate combining [33], [35], with a corresponding increase in directivity. The radiation pattern is narrower than for the passive array because of the nonlinearity of the rectifier, as shown in both simulations and measurements in [49]. An example single-element radiation pattern is shown in Fig. 4 for a patch rectenna at 1.96 GHz [50]. This reduces the energy harvesting efficiency for nonstationary sources, as discussed in Section V. In broadband arrays, the element spacing is small compared to the wavelength at lower frequencies and the radiation pattern less directional.

The dc collection circuitry is an important part of array design, as is the power management circuit that needs to be efficient at very low power levels [22]. Connecting the dc outputs in a reconfigurable manner in [23] was shown to enable peak efficiency tracking for a range of optimal dc loads from 10 Ω to 5 k Ω , for a range of incident power levels from 5 to 50 $\mu\text{W}/\text{cm}^2$ [24]. A more comprehensive discussion of RF and dc combining is given in [51] in this issue.

C. Rectenna Array Efficiency

The key performance metric is conversion efficiency, $\eta_{\text{RF-dc}} = P_{\text{dc}}/P_{\text{RF,in}} = \eta_{\text{RF-dc}}(f, P_{\text{RF,in}}, R_L)$, where R_L is the dc load resistance. Assuming that the effective area of the integrated rectifier antenna is the largest possible, equal to the geometric area, A_G , the expression becomes

$$\eta_{\text{RF-dc}} = \frac{V_{\text{dc}}^2}{R_L} \cdot \frac{1}{S(0^\circ, 90^\circ) \cdot A_G} \quad (1)$$

where $S(0^\circ, 90^\circ)$ is the power density incident from broadside. The denominator in (1) overestimates the RF power delivered to the diode; therefore, the efficiencies reported in this way are conservative lower bounds and can be precisely calibrated in a measurement for normally copolarized incident powering waves. Other efficiency definitions have been reported in the literature. For example, in [55]

and [56], $P_{\text{RF,in}}$ is based on the Friis formula, and the efficiency is found from

$$\eta'_{\text{RF-dc}} = \frac{V_{\text{dc}}^2}{R_L} \cdot \frac{(4\pi r)^2}{P_T \cdot G_T \cdot G_R \cdot \lambda^2} \quad (2)$$

where P_T , G_T , and r are the transmitted copolarized power, gain, and distance of the transmitter, and G_R is found from measurement or simulation of an equivalent antenna without the rectifier. This definition does not take into account the nonlinear loading of the antenna by the feed, coupling between the rectifier and antenna, mismatch, and ohmic losses. Small errors in r , G_T , P_T , or G_R have a large effect on the resulting η' . Another definition in the literature, for example, [54], uses measured power density at the integrated rectifier antenna plane and estimates the effective area of the antenna obtained through gain measurement or simulation

$$\eta''_{\text{RF-dc}} = \frac{V_{\text{dc}}^2}{R_L} \cdot \frac{1}{S(0^\circ, 90^\circ) \cdot A_{\text{eff}}} \quad (3)$$

As in (2), the antenna gain is found for a fixed (usually 50- Ω) load and does not take into account gain changes due to nonlinear rectifier loading. The difference between η' and η was found to be as large as 10% points, where η' overestimates the actual efficiency.

Section III introduces a 10-GHz narrowband array with RF combining, with the goal of showcasing an interesting application and providing a contrast to broadband arrays that are the focus of the remainder of this article.

III. 10-GHz SCALABLE RECTENNA HARVESTING ARRAY

A narrowband 10-GHz array for ground-based harvesting CP satellite transmitters is shown in Fig. 5, with RF combining of $M = 16$ patch antenna elements at each rectifier. In this section, a “unit cell” is defined as a set of four patch elements that share a sequential feed network (see Fig. 6). Following the aforementioned naming convention, the array outlined in white dashed line in Fig. 5 is considered a 2×2 square array, and nine of these are arranged in a square since the approach is modular. Here, we show results on a 1×4 linear array and a 2×2 square array, each consisting of four unit cells. A Skyworks SMS7630-079LF Schottky diode with package parasitics provided in [55] for an SOD523 package is source-pulled in simulation and measurement, with a resulting impedance of $Z = 8 + j13.5 \Omega$ at the diode plane, obtained for -30 - to 0 -dBm available source power. A simple matching network consisting of a 50- Ω 50 $^\circ$ shunt stub and 50- Ω $\lambda_g/4$ line with a 0.3-pF shunt capacitor matches the diode impedance to 50 Ω . Fig. 6 shows the realized matching network as part of the integrated rectenna [33]. The dc output power is measured across a variable resistive load placed in parallel with the capacitor.

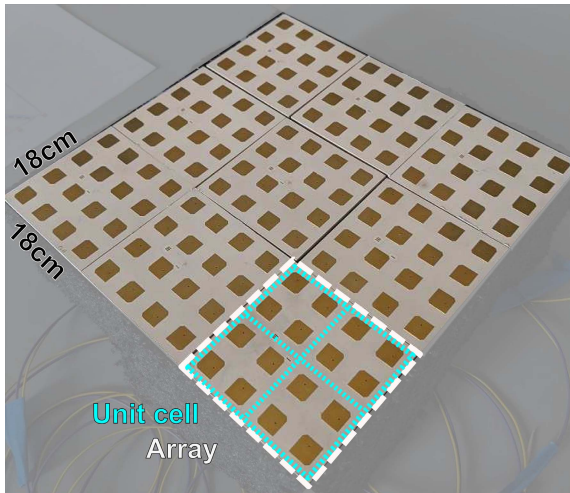


Fig. 5. Photograph of a 10-GHz harvesting array with RF combining at the 16-element level. The array consists of four unit cells with a shared dc load. Foam backing is included for structural support.

Measured RF-dc conversion efficiency for varying input power levels and dc loads swept from 300Ω to $3 \text{ k}\Omega$ is shown in Fig. 7, along with a sixth-order polynomial model of the efficiency envelope. Section V utilizes this polynomial model to determine theoretical rectified output power for an arbitrary rectenna array topology. The inset image in Fig. 7 shows example source-pull contours for conversion efficiency and output power taken at 10 GHz with -10 dBm of incident RF power. The maximum RF-dc conversion efficiency is approximately 20%. The dc load that results in the highest efficiency varies with incident power on the diode, and it can be observed that the efficiency exhibits greater variation as a function of dc load at higher power levels. An extended discussion on ideal dc loading as a function of the incident power is provided in [33].

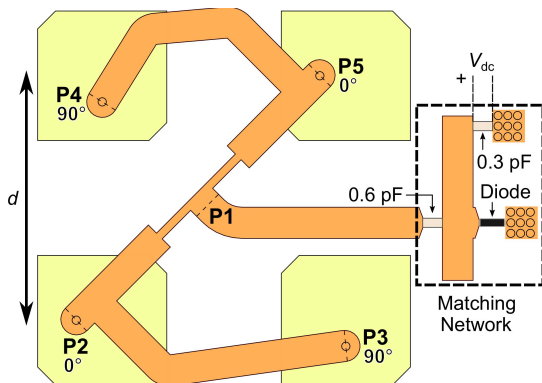


Fig. 6. Layout of unit cell with integrated matching network. Patch elements (lighter) are located on the top and sequential feed and matching network (darker) on the bottom layer of the substrate. The center-to-center element spacing is $d = \lambda_0/2$.

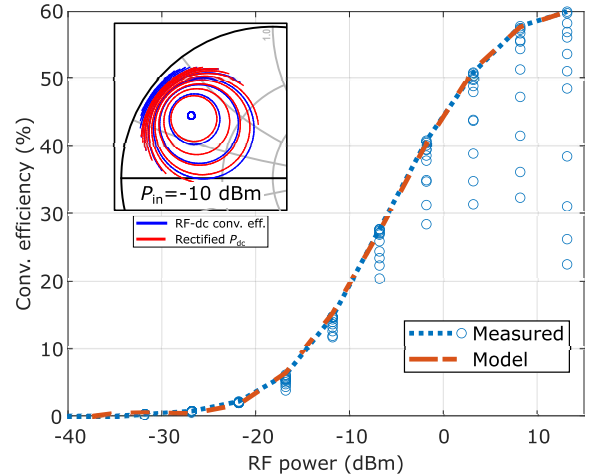


Fig. 7. Modeled and measured rectifier efficiency as a function of RF power for varying dc loads. Inset: source-pull contours for $P_{RF} = -10 \text{ dBm}$ and $\eta_{\max} = 20\%$. The orange curve traces the maximum measured efficiency envelope, while the blue dots represent efficiency for different dc loads, from 300Ω to $3 \text{ k}\Omega$.

To increase input RF power to the rectifier and achieve circular polarization, the subarray has a sequential feed network with progressive phase shifts and equal power division [56], as shown in Fig. 6, with port 1 as a reference plane for the diode matching network. For scalability at the array level, the spacing is constrained since the feed must be contained within the patch subarray footprint. With this in mind, ideal power division and phase response are difficult to achieve. Simulations show that a maximum amplitude imbalance of 1 dB results from the added loss at ports 3 and 4 relative to ports 2 and 5. The simulated phase difference between ports 2 and 5 is under 4° , while quadrature ports 3 and 4 deviate $+7^\circ/-9^\circ$ from the nominal -270° , respectively. This phase and amplitude imbalance degrades the axial ratio.

In order to demonstrate scalability, two rectenna arrays are designed—one in a 2×2 planar/square lattice and the other in a 4×1 linear array—and compared in terms of dc output power and RF-dc conversion efficiency as a function of incident power density at boresight. The measured data are shown in Fig. 8. The 2×2 combined array shows an increase in conversion efficiency over that of both the unit cell and 4×1 array for all power densities. Maximum efficiency for the former approaches 20% for $100 \mu\text{W}/\text{cm}^2$ incident power density, while the linear array and subarray are between 15% and 16%, respectively. A nonzero conversion efficiency at very low power densities for the array is due to a lack of measurement averaging. The benefit of power-combining is clear: at $100\text{-}\mu\text{W}/\text{cm}^2$ incident power density, the 2×2 array produces above -4 dBm of dc power compared to the subarray output of -10 dBm or a 6-dB relative increase in output power. At the lowest power density, this relative increase exceeds 10 dB.

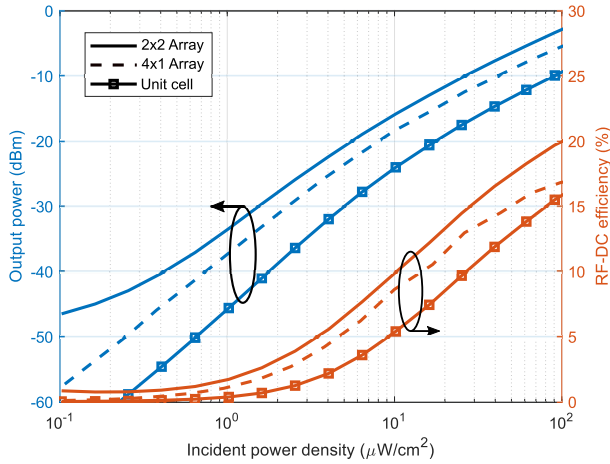


Fig. 8. Measured RF-dc conversion efficiency and dc output power for various array/unit cell designs.

To provide a fair comparison, however, the physical size of the rectenna array must be taken into account. Each array has a footprint of approximately 36 cm^2 , while the unit cell is 20 cm^2 , or 80% smaller in size; however, the 2×2 power-combined array produces a factor of 4 higher output power compared to the unit cell. Thus, there is a clear benefit in RF power combining for low incident power densities. To examine the effect of the dc load on rectenna performance, a variable load is swept from 500 to 3 k Ω while simultaneously varying incident power density from 0.1 to 130 $\mu\text{W}/\text{cm}^2$ at 10 GHz. While a maximum conversion efficiency slightly above 16% is measured for a dc load of 750 Ω at maximum power density (for a unit cell), the ideal dc load is shown to increase toward, or exceed, 3 k Ω for decreasing power densities, indicating that series dc combining is preferred.

An extension of RF and dc combining described above, and similar to the dc combining for a 2-GHz array in [23], was recently demonstrated in a modular X-band rectenna array with voltage- and current-summing “tiles” (i.e., a collection of unit cells) [57]. In this work, each tile possesses six rows of six series rectenna unit cells. While each row sums the dc currents from the cascade unit cells, the differential outputs of each row connect in series to sum the dc voltages. This effectively produces a 36-fold increase in rectified dc output power compared to that of a single unit cell, assuming uniform illumination. Scaling of this topology is further demonstrated to cover a $1 \times 1.1 \text{ m}^2$ array footprint, with rectified dc power exceeding 16 dBm with an incident power density of 92 $\mu\text{W}/\text{cm}^2$ up to 30° off broadside.

IV. BROADBAND RECTENNA ARRAYS

Broadband rectenna arrays with spacings much less than half of a free-space wavelength over most of the operating range should ideally present a $377\text{-}\Omega/\square$ surface impedance to incident plane waves. Two geometries are

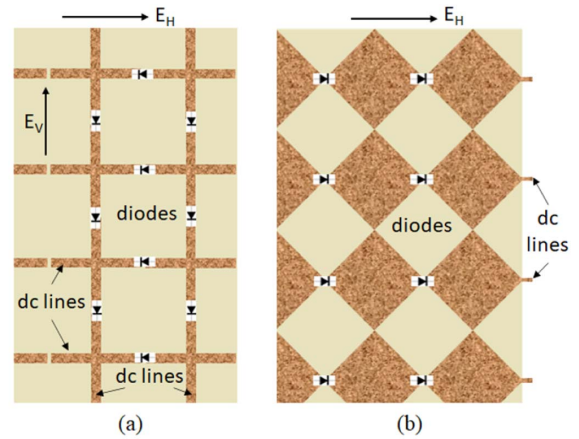


Fig. 9. (a) Dual-polarized grid rectenna [44] and (b) bow-tie array with diodes connected in the horizontal polarization direction [38], [39].

shown in Fig. 9. The grid rectenna receives both linear polarizations, and the rectified dc currents are all combined [see Fig. 9(a)]. The bow-tie array [see Fig. 9(b)] is self-complementary if in air and infinite in extent, with a broadband impedance at each port of $(377^2/4)^{1/2} = 189 \Omega$. Although, in principle, diodes can be connected along with both horizontal and vertical directions, in the published bow-tie rectenna arrays [38], [39], the diodes are only connected in one direction. It is interesting that measurements show that, for finite bow-tie arrays larger than 4×4 , this still results in comparable dc power for both horizontal and vertical incidences.

Another self-complementary and broadband antenna element is an infinite spiral, suggesting broadband behavior in an array environment, Fig. 10. For a bandwidth comparison, a grid array and a spiral array operating

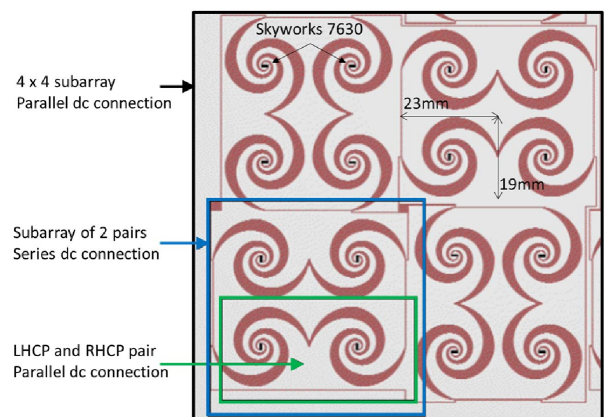


Fig. 10. Dual circularly polarized spiral 4×4 rectenna subarray, four of which are combined in a 8×8 array with reconfigurable dc combining [37].

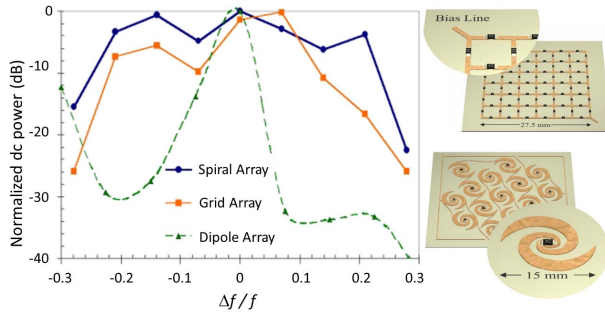


Fig. 11. Measured fractional frequency bandwidth of normalized dc power delivered to an optimal load for the grid rectenna array (orange line, geometry shown in top inset), spiral array (blue line), and linear eight-element resonant dipole array (dashed green line). The response is measured with an incident CP wave at boresight [44].

in the 4–6-GHz range are compared in [44], and their measured fractional bandwidths, compared with resonant dipole array at the center frequency, are shown in Fig. 11. Defining the bandwidth to be at -10 dB of the peak received dc power, the dipole, grid, and bow-tie arrays show fractional bandwidths of 10%, greater than 30% and 50%, respectively. In the remainder of this section, some interesting results for spiral and bow-tie arrays are discussed.

A. Example Spiral Rectenna Array

Spiral rectenna arrays are among the first harvesting arrays to be investigated [37], [44]. Fig. 10 shows a 16-element subarray, or quartile, of a 64-element spiral rectenna array characterized over nearly a decade bandwidth, from 2 to 18 GHz.

The measured broadband frequency response for various incident power levels for the full 64-element array is shown in Fig. 12. The measured receive gain of the array at dc is used to relate the data to the power density by $P_r/G_r = S\lambda^2/(4\pi)$. Some power is rectified from ambient RF radiation in the building, shown as shaded. The inset shows the source-pull impedance range for best conversion efficiency of the Skyworks SMS7630 Schottky diode as frequency and input power vary between 1 and 16 GHz and -30 and 10 dBm, respectively. Matching to antenna impedance over this range is performed with the spiral element, but not optimally. The individual elements are coupled tightly at the lower edge of the band (at 2 GHz, the array period about $0.15\lambda_0$), while not much coupling is expected at the higher end of the band (at 18 GHz, the element spacing is about $0.7\lambda_0$).

For a broadband array, harmonics of the fundamental fall into the operating range. Reflected fundamental-frequency power and reradiated harmonic power from the nonlinear rectification process for the 64-element spiral array at an incident fundamental frequency at 3.4 GHz

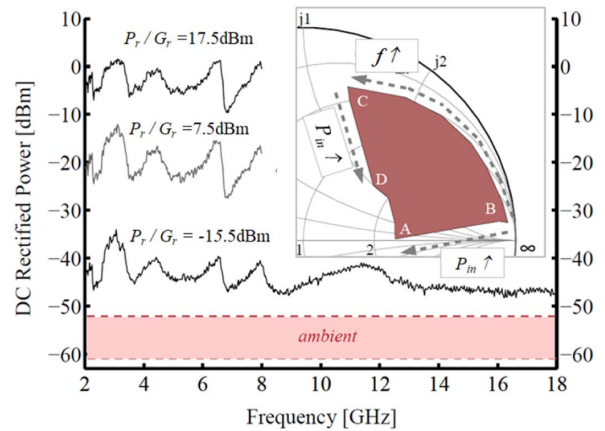


Fig. 12. Measured broadband frequency response for various incident power levels related to the power density by $P_r/G_r = S\lambda^2/(4\pi)$. The shaded area represents the range of rectified power levels resulting from ambient RF background signal present in the building. The inset shows the source-pull impedance range for best conversion efficiency of the Skyworks SMS7630 Schottky diode as frequency and input power vary between 1 and 16 GHz and -30 and 10 dBm, respectively.

are measured over a range of linearly polarized incident power densities and presented in Fig. 13. It is remarkable that there is measurable harmonic reradiation when the incident power density on the array is as low as $1 \mu\text{W}/\text{cm}^2$.

In the 81-element array, four quartiles from Fig. 10 have the ability for dc reconfiguration. The dc combining in series and parallel results in efficiencies at the center of the band ranging from 13% (all in series) to 20% (all in parallel) for an incident power density of $60 \mu\text{W}/\text{cm}^2$. When the elements are in series, the dc Thevenin resistance is higher

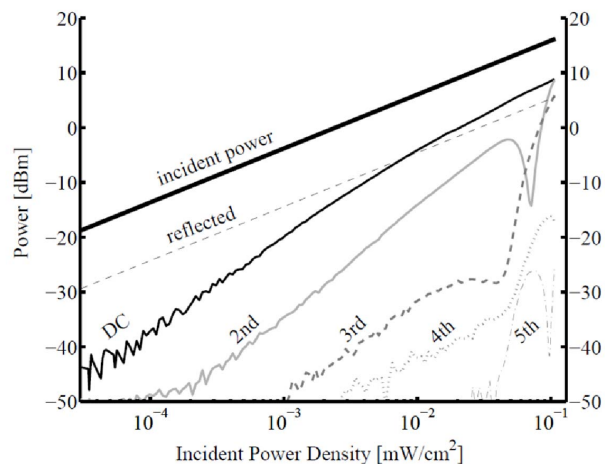


Fig. 13. Measured reradiated fundamental ("reflected") and harmonics from a 64-element spiral array with incident fundamental frequency at 3.4 GHz over a range of incident power densities with a $100\text{-}\Omega$ dc load.

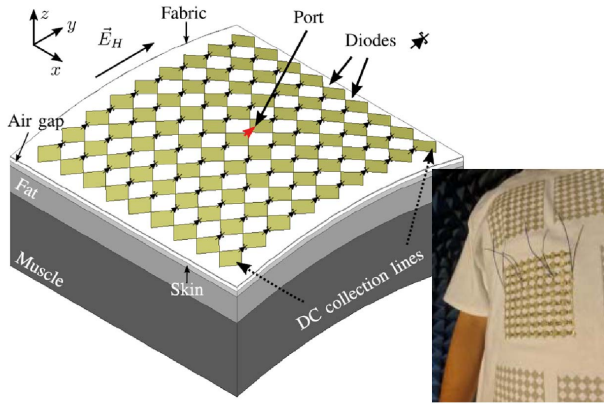


Fig. 14. Sketch of layers included in simulations for the case of the OB rectenna array, with inset showing a photograph of the tee-shirt worn by one of the authors during OB measurements.

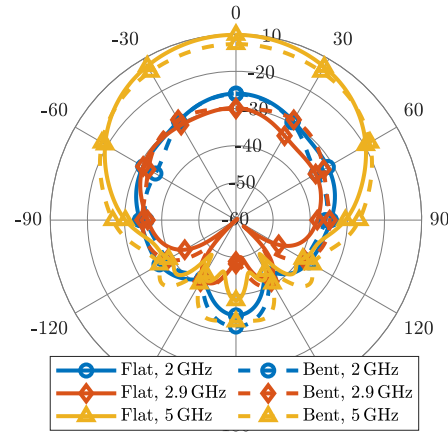


Fig. 16. Comparison of realized gain at three different frequencies (2, 2.9, and 5 GHz) for flat and curved array in the horizontal polarization.

than the 600-Ω dc load used in the measurements. The array efficiency is significantly higher than that of a single quartile (<1%), showing that the dc and RF combining improve efficiency at low power levels.

B. Example Bow-Tie Array

Bow-tie arrays of 16 and 81 elements shown in Fig. 14 are designed for harvesting 2–5-GHz 5G signals and are screen-printed on a cotton tee-shirt [39], [45], using conductive ink. Skyworks SMS7630 diodes are connected at the feed points with added silver paint. A similar source pull to the inset of Fig. 12 is performed, with resulting impedances shown in Fig. 15; the trends with varying load resistance and frequency are shown with arrows.

The bow-tie wearable array from Fig. 14 is simulated using Ansys HFSS and CST, including the curvature of the body and realistic parameters of the tissues given in [39].

Simulations of the realized gain radiation pattern with and without the body curvature are shown in Fig. 16, indicating that bending does not affect the radiation pattern or impedance significantly. Two arrays are simulated, fabricated, and characterized to investigate scaling—4 × 4 and 9 × 9 arrays on the same cotton material and using the same fabrication technique. The diodes are connected along with the horizontally polarized feeds, as shown in Fig. 9. The period of the arrays is 1.25 cm, which is less than $\lambda_0/6$ at the highest operating frequency of 5 GHz. This means that the elements are tightly coupled, and simulations with all other elements loaded are required to find the impedance presented to each diode, as described in detail in [39].

The arrays are characterized in an anechoic chamber both on a water phantom (Ph) and on a human body (coauthor and graduate student at the time). The power density at the plane of the array is calibrated with two identical broadband ridge horn antennas. The optimal measured dc load resistance and rectified power are examined as a function of incident power density and frequency, and the results are shown in Fig. 17. Note that the optimal load generally increases with increasing frequency and with decreasing incident power density. The rectified power profile shows the expected decrease in efficiency at very low input power density and at higher frequencies. Fig. 18 summarizes the performance over input power at the edges of the frequency band, 2 and 5 GHz, showing the range in optimal dc load and output dc power.

The measured rectified power with a 2-kΩ dc load with incident copolarized (horizontal) and cross-polarized (vertical) radiation is shown in Fig. 19 for the 81-element tee-shirt array on a water Ph and on-body (OB). The results are consistent with previous bow-tie rectenna measurements, e.g., [38]—although the rectifiers are connected to the horizontally polarized feeds, both linear polarizations are received and rectified.

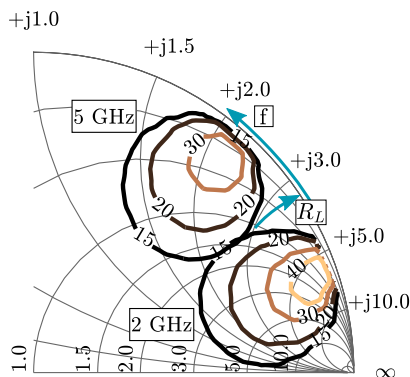


Fig. 15. Simulated source-pull results showing contours of constant rectified power (in μW) at 2 and 5 GHz with an input power and dc load of 100 μW and 2 kΩ, respectively. The location trend for the optimum load and frequency (f) and load (RL) is shown with arrows. The loads are varied from 100 to 5 kΩ.

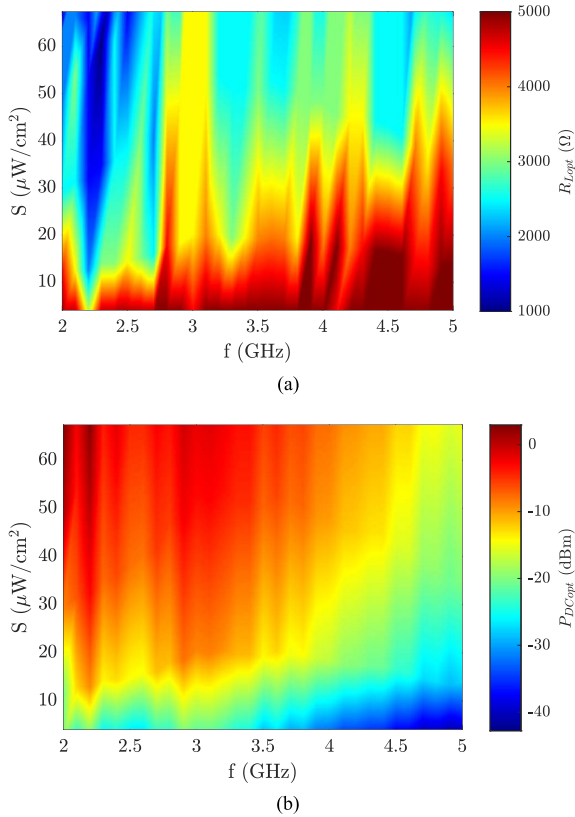


Fig. 17. Measured optimal (a) load resistance and (b) dc output power for the 81-element array with the incident electric field in the horizontal polarization, as a function of frequency and incident power density. The output powers in (a) correspond to the load resistances in (b).

The scaling of the tightly coupled screen printed array is investigated through a comparison between a smaller 16-element array and a larger 81-element array. The relevant conclusions are summarized in Fig. 20. Conversion efficiency, defined as $\eta''_{\text{RF-dc}} = P_{\text{dc}}/S \cdot A_G$, results in a conservative efficiency estimate and is plotted in Fig. 20

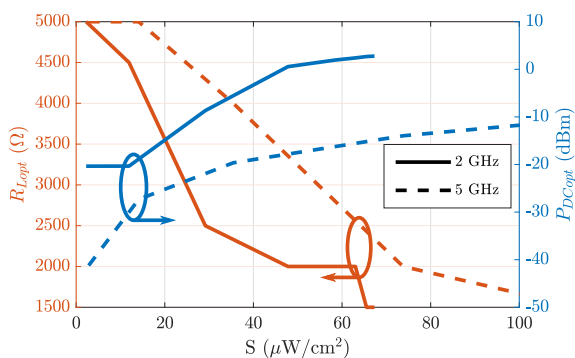


Fig. 18. Measured optimal load resistance and output power for the 81-element array with a horizontally polarized incident wave at the edges of the band, 2 and 5 GHz, with varying incident power density.

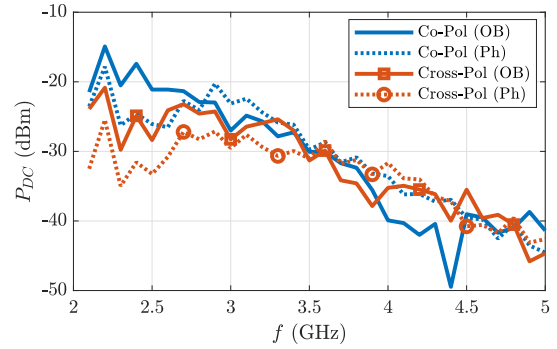


Fig. 19. Rectified dc power versus frequency for the 81-element array measured OB and with Ph with horizontal (Co-Pol) and vertical (cross-Pol) polarizations. The incident power density is $4 \mu\text{W}/\text{cm}^2$, and the dc load is $2 \text{ k}\Omega$.

for the two array sizes for the horizontal polarization at the center frequency of 2.9 GHz. The voltage is measured across a 2-k Ω load. The larger array does not produce significantly higher power compared with the smaller array. It is believed that the efficiency drops due to the relatively high dc resistivity of the conductive ink, which becomes more dominant as the array is scaled up in size. These results indicate that, in terms of efficiency, it is better to combine the power of several small arrays than to create a single large array.

V. APPLICATION SCENARIOS

The arrays described above are designed for specific scenarios. For example, the wearable array is designed to harvest communication signals in the sub-6-GHz 5G band. For it to be practical, it needs to survive folding and washing. After coating the silver paint with nail polish and hand-washing the shirt, the diode current is measured and compared in [39]. The 2–18-GHz spiral array is designed to harvest a wide range of modulated signals simultaneously and is, therefore, examined in a statistical multisignal scenario. The ground-based 10-GHz array is

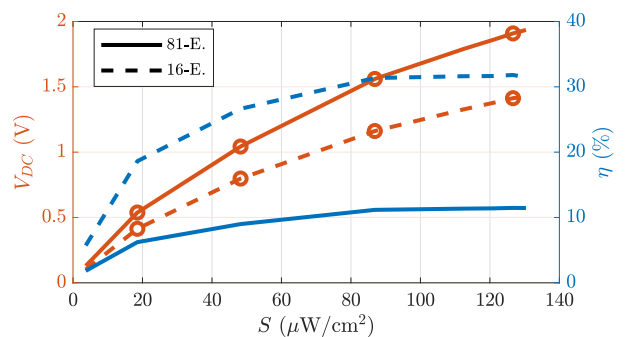


Fig. 20. On-Ph measurement results of efficiency and output dc voltage (circles) versus incident power density at 2.9 GHz with a dc load of $2 \text{ k}\Omega$. The fairly large resistance of the conductive ink reduces efficiency for larger arrays while providing larger voltages.

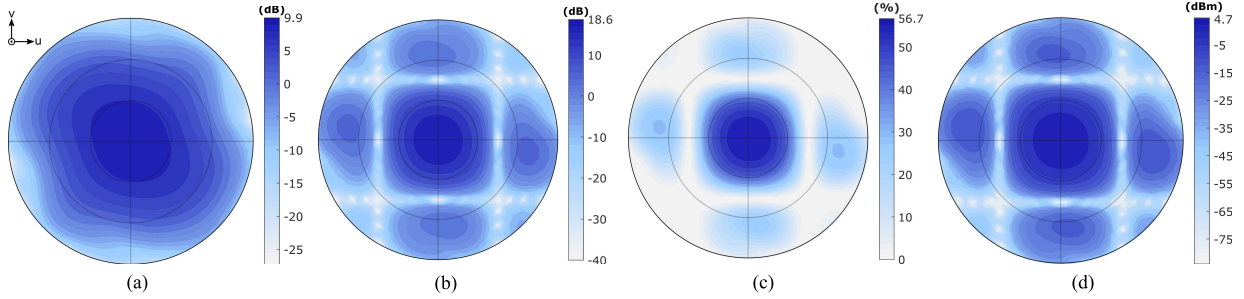


Fig. 21. Workflow for estimating rectified output power of a given RF-harvesting array topology. (a) User-defined unit cell (unit cell gain) is arrayed in a 2×2 square lattice with $d_x = d_y = \lambda_0$, and (b) theoretical gain (array gain) is determined. Upon mapping the diode efficiency model to the calculated aperture with a provided incident power density, (c) RF-dc conversion efficiency and (d) dc output power (rectified P_{dc}) can be plotted. The patterns are defined and plotted in u - v space for hemisphere $z \geq 0$, assuming that the array lies in the xy plane.

intended to receive low power from a known satellite transmitter in energy-denied environments to enable basic communications functions. As such, its performance over azimuth and elevation is relevant and is described next.

A. Space-to-Earth Power Transfer

In the context of space-to-Earth power transfer where the microwave transmitter is on a satellite in low Earth orbit (LEO) and the receiver is mounted to a stationary, nontracking platform, we seek to determine the ideal array structure, which will maximize the amount of rectified output power. The following analysis will introduce a methodology for comparing various rectenna array topologies and their theoretical output powers, given an LEO-based transmitter with arbitrary and unknown trajectory over the array.

First, either a measured or simulated model is generated for the rectifying element. In this example, we use a polynomial model of measured rectifier efficiency as a function of incident RF power for the Skyworks SMS7630-079. A model of order $N = 6$ is generated using MATLAB's Curve Fitting Toolbox [58]

$$\eta(x) = a_0 + \sum_{n=1}^N a_n x^n$$

where $a = \{44.66, 2.291, -6.576 \times 10^{-2}, -3.748 \times 10^{-3}, 8.527 \times 10^{-5}, 5.275 \times 10^{-6}, 5.706 \times 10^{-8}\}$. As previously mentioned, η is RF-dc conversion efficiency, and x represents the input RF power. This polynomial is shown by the dashed orange line in Fig. 7, and a good agreement is seen with measured data. There are multiple instances in which the model predicts negative efficiency for very low power levels; this nonrealizable value is forced to zero in postprocessing.

Following creation of the diode model, an antenna unit cell is selected. In this instance, the unit cell is defined in Figs. 5 and 6. A full-wave simulation of unit-cell gain is shown in Fig. 21(a), and boresight measurement data can be found in [33]. Maximum realized gain is approximately 9.9 dB with slight main lobe asymmetry exhibited

due to unequal power distribution in the sequential feeding network. The coordinate system is similar to that in [59], with the center of each plot representing $(\theta = 0^\circ, \phi = 0^\circ)$. The azimuth angle ϕ increases counterclockwise from 0 – 360° , while the elevation angle θ increases radially from 0° to 90° .

For scalability purposes, a planar rectenna array is developed, with the standard array factor (AF) given by

$$AF(\theta, \phi) = \sum_{m=1}^M e^{j(m-1)(kd_x \sin \theta \cos \phi + \beta_x)} \cdot \sum_{n=1}^N e^{j(n-1)(kd_y \sin \theta \sin \phi + \beta_y)} \quad (4)$$

where $[M, N]$ are the number of elements along the x - and y -axes, d is the element spacing, and $\beta_{x,y}$ is the progressive phase shift between elements along a given axis. Mutual coupling is not taken into account but may be necessary for large array sizes [60]. Directivity of the AF is calculated using

$$D = \frac{4\pi [AF(\theta, \phi)]^2}{\int_0^{360^\circ} \int_0^{180^\circ} [AF(\theta, \phi)]^2 \sin \theta d\theta d\phi}. \quad (5)$$

An example topology is selected with parameters $d_x = d_y = \lambda_0$, $\beta_x = \beta_y = 0^\circ$ in a 2×2 square configuration. By substituting (4) into (5) and mapping its result to the gain profile shown in Fig. 21(a), theoretical array gain can be determined. Array gain for the previously mentioned topology is shown in Fig. 21(b). Maximum gain is calculated to be 18.6 dB. For presentation purposes, a gain floor of -40 dB is imposed.

Upon determining the array gain, one can calculate an effective aperture. In knowing or assuming the incident power density on the array (in this example, we choose $100 \mu\text{W}/\text{cm}^2$), the calculated aperture can be applied to determine incident RF power. In this example, feed network and matching network losses are neglected. It is then straightforward to estimate the RF-dc conversion efficiency for the rectenna array given that we now have

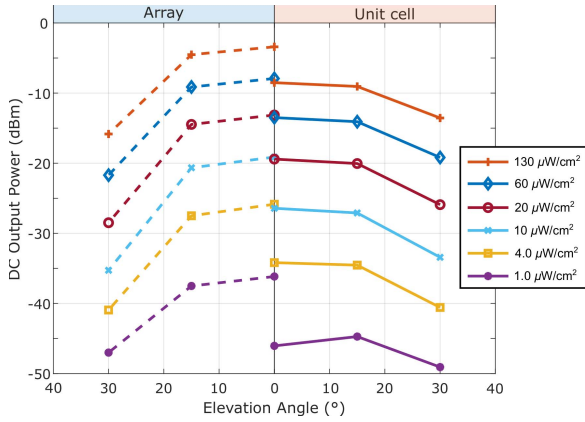


Fig. 22. DC output power as a function of angle of incidence for a 2×2 power-combined array and unit cell.

an accurate diode model and estimated incident RF power on the rectifying element. This conversion efficiency and, thus, theoretical rectified P_{dc} can be displayed as spatially varying patterns, as shown in Fig. 21(c) and (d), respectively.

Due to the ultralow power density produced by the transmitter satellite in the given scenario, both mechanical and active electronic tracking techniques are not economical. Therefore, the designer must consider rectenna performance across arbitrary satellite trajectories/azimuths relative to the rectenna array. Fig. 22 shows calculated RF-dc conversion efficiency as a function of elevation angle for two incident power densities. The shaded regions represent all cuts in ϕ , while the dashed lines indicate worst and best case performances for a given elevation. Using these power and efficiency patterns for any known rectenna array, average power can be integrated across an orbital period to determine whether or not the topology of interest is capable of supplying enough energy to power a low-duty cycle sensor. Care should be given to ensure that integrated power is compared for a normalized “panel” size, i.e., a single power-combined array is compared to N unit cells of equivalent size/footprint.

Fig. 22 shows a relative comparison in dc output power for angles of incidence up to 30° off broadside for both a 2×2 power-combined array and unit cell. While the benefit of power combining for broadside incidence is apparent, the combined array exhibits a narrower beamwidth compared to that of the unit cell, thus producing lower rectified output power at larger angles of incidence.

B. Multitone Broadband Power Harvesting

In a harvesting scenario, multiple signals may be incident simultaneously. More than two decades ago, researchers realized that multiple simultaneous signals may improve conversion efficiency [44]. Fig. 23 shows

measured normalized dc power for a vertically polarized incident wave on the 16-element spiral array from Fig. 11 at 8.5 GHz (circles), at 12.2 GHz (squares symbols), and for waves at both frequencies simultaneously (dashed). In the latter case, the measured dc power is increased by 3 to 5 dB over the simple sum of the first two cases.

Applying two simultaneous CW signals, f_1 and f_2 of equal power $P_1 = P_2$ are equivalent to applying a signal of instantaneous bandwidth $|f_1 - f_2|$ with a 3-dB peak-to-average power ratio (PAPR). For example, in the case from Fig. 23, the signal instantaneous bandwidth is 3.7 GHz. For N equal-power signals, $\text{PAPR} = 10 \log 2N$ (9 dB for four signals). Rectification of multisine signals with high PAPR is investigated for closely spaced signals with a simple theory and simulations in [61] and extended to harmonically spaced signals in [62]. Another experimental investigation of the improvement in the efficiency of closely spaced sine waves is shown in [63], and the propagation environment is considered in [64]. A theoretical treatment at the MIMO communication system level in [65], using a very simple rectifier model, shows that joint multisine waveform and beamforming design can improve conversion efficiency. Modulated signals with different PAPRs, including chaotic signals, with a >400 -MHz aggregate bandwidth, are analyzed experimentally in [66] and [67].

In terms of rectifier theory for multiple signal excitation, a Taylor expansion of the I - V curve of a diode is used, without taking into account the resistance of the diode, e.g., [61]. This resistance is the main contributor to inefficiency at low power levels and results in a more complicated relationship [68]

$$I(V, I) = I_s \left(e^{(V - IR_s)/nV_T} - 1 \right) \quad (6)$$

where R_s is the series resistance of the diode, I_s is the saturation current, and $V_T = kT/e$. The expansion of this equation is done using Wright omega functions in [68].

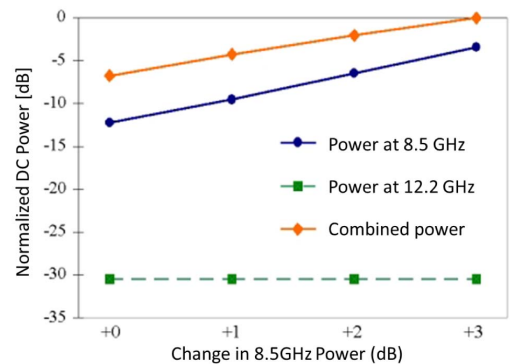


Fig. 23. Measured normalized dc power for a vertically polarized incident wave on the 16-element spiral array in Fig. 11 at 8.5 GHz (circles), at 12.2 GHz (squares symbols), and for waves at both frequencies simultaneously (dashed). In the latter case, the measured dc power is increased by 3–5 dB over the simple sum of the first two cases.

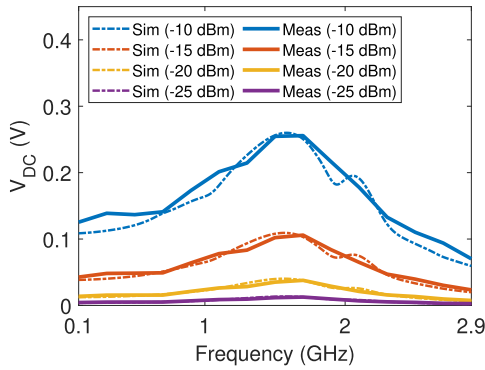


Fig. 24. Extracted Skyworks SMS7630 diode model validated in a rectifier circuit over a broad bandwidth and over a range of low input power levels.

When no bias is applied to the diode (harvesting case), the current can be written as a power series in applied voltage V , where the coefficients are written in terms of Wright omega functions. A multitone signal voltage can then be applied and the resulting rectified current analyzed.

The theory for the simple resistive diode shows improvement with multiple tones, so a broadband rectifier is designed to cover 0.9–3.35 GHz. The Skyworks diode model did not predict the measured broadband behavior, so an improved nonlinear model was extracted and validated against measurements of a rectifier matched to 50 Ω . The agreement between the simulated and measured rectifier performance over frequency and input power is shown in Fig. 24. A setup is designed for multifrequency testing with up to four simultaneous tones, with a Wilkinson combiner network covering 1–3 GHz. An example measurement comparing two simultaneous incident signals to the individual signals with equal average power is shown in Fig. 25. Note that the comparison is between the multitone and individual signals at double the power, not the separate sum of equal-power individual tones. Since the rectifier does not behave uniformly over frequency, there are cases when the two-tone output is lower than one of the individual stronger signals, which is predicted by the simple theory in [68].

An alternative comparison is a multitone dc response compared to the sum of the individual tone responses. An experiment with the 64-element spiral array in a controlled two-tone environment is performed, with the two tones between 2 and 8 GHz having different powers, resulting in a range of PAPR values. The instantaneous bandwidth of the incident signal at each rectifier is equal to the difference in the frequency of the two tones and is up to 6 GHz wide. Two signal sources, separated by 20° in incidence angle from the rectenna and 45° in polarization, are used to produce multiple incident waves with variable frequency and power. In order to ensure uncorrelated inputs, paired frequencies and power levels are generated randomly with a uniform distribution. The experiment is

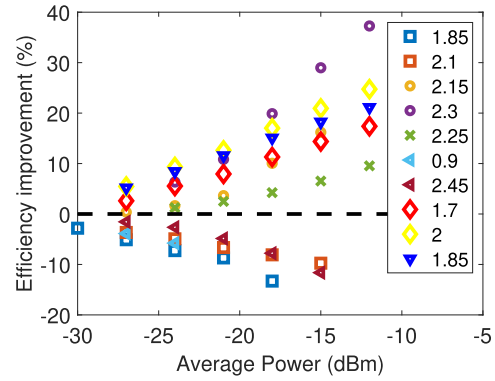


Fig. 25. Measured rectified power with an optimal load for sets of two simultaneous tones of equal total average power compared to the dc output when one tone of the same total power is applied. Each set of two simultaneous tones is indicated with the same symbol; colors denote specific frequencies.

run by first generating one randomized frequency between 2 and 8 GHz and one incident power level between approximately 0.1 $\mu\text{W}/\text{cm}^2$ and 0.1 mW/cm^2 . Each source is turned on separately, and independent dc rectified powers are recorded. Both sources are then turned on simultaneously as a multitone signal. This process is repeated for 10 000 randomized input pairs $[(f_1, P_1); (f_2, P_2)]$. The sums of the two independent rectified powers for each trial were then sorted and compared with the corresponding rectified power from the simultaneous illumination from both sources.

The result of this statistical test is shown in Fig. 26. In all 10 000 cases, the multitone rectified power is higher than the sum of individual tones, and the improvement in efficiency is larger at lower incident power levels. Three distinct regions with about 60%, 40%, and less than 30% enhancement are identified for an incident power range between 0.1 and 100 $\mu\text{W}/\text{cm}^2$.

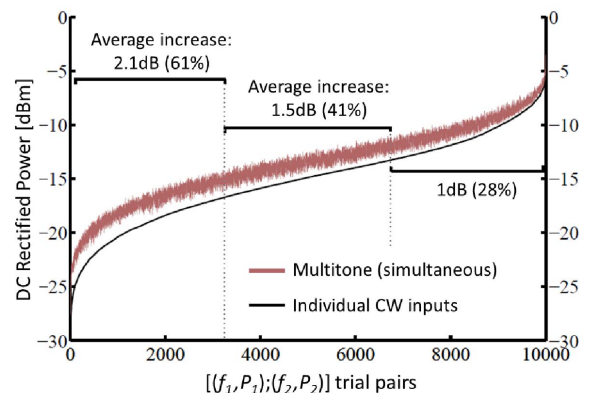


Fig. 26. Comparison of total rectified power for independent and simultaneous dual-frequency illumination of the 64-element 2-18-GHz spiral array, measured with tones between $f_1 = 2$ GHz and $f_2 = 8$ GHz, as explained above. The results of 10 000 trials are rank-ordered by dc rectified power to illustrate the power-dependent increase in rectification efficiency.

VI. CONCLUSION

For RF energy harvesting, broadband rectenna arrays offer scalable dc power from one or more wireless sources. In this article, we first compare the design methodology and scalability of narrowband and broadband arrays. An example 10-GHz array with RF combining showcases the challenges involved in ultralow-power (down to $1 \text{ mW/m}^2 = 0.1 \text{ } \mu\text{W/cm}^2$) harvesting of a known narrowband signal. The circularly polarized array consists of subarrays with RF power combining before rectification. This approach is contrasted to harvesting over a wide RF bandwidth, through a comparison of several broadband arrays with rectifiers in each element. This includes a 2–5-GHz bow-tie screen-printed wearable rectenna array with an efficiency exceeding 30% above $50\text{-}\mu\text{W/cm}^2$ incident power density and a 2–18-GHz spiral array tested with powers down to $0.1 \text{ } \mu\text{W/cm}^2$.

In terms of types of harvested signals, the narrowband array is analyzed in the context of its application for a ground-based directional harvester of an LEO satellite transmitter in an energy-denied environment. Broadband arrays are analyzed with multiple widely spaced simultaneous signals, confirming efficiency enhancement when the input signal on the rectifier has a high PAPR and wide instantaneous bandwidth.

In summary, the field of RF energy harvesting has seen a lot of developments in the last two decades. Due to the continuously expanding use of the EM spectrum, harvesting efficiently over a broad RF bandwidth will become increasingly important, and the broadband

examples described in this article show some possible approaches to achieving multioctave bandwidths. Designing RF harvesters for modulated signals instead of CW waveforms will be more relevant as emerging communications signals have increased instantaneous bandwidths and PAPRs to meet capacity requirements. For low power densities, harvesting power over a large area with new types of flexible and even transparent substrates leads to conformal rectenna array solutions that have not been investigated much to date. Furthermore, since Schottky diodes have a finite turn-on voltage, for very low power levels, this limits harvester efficiency, operability, and startup; new types of rectifying devices, such as tunnel diodes, could make a substantial impact. Although integration with power management circuits has been shown by a number of authors, integration of harvesters into either existing or new communications and sensing systems will remain an interesting and useful avenue of both research and engineering of RF harvesting arrays. ■

Acknowledgment

The authors would like to thank Dr. Chris Rodenbeck at the Naval Research Laboratory (NRL), Prof. Taylor Barton at the University of Colorado Boulder, Prof. Daniel Segovia at the University Carlos III of Madrid, and Mónica Borgoños-García. Special thanks to Dr. Joe Hagerty for pioneering work and many helpful discussions on wireless power transfer (WPT). Modelithics models utilized under the University License Program from Modelithics, Inc., Tampa, FL, were used in designs.

REFERENCES

- [1] W. Zhong, D. Xu, and R. S. Y. Hui, *Wireless Power Transfer: Between Distance and Efficiency*. Singapore: Springer, 2020.
- [2] N. Shinohara, *Recent Wireless Power Transfer Technologies Via Radio Waves*. Gistrup, Denmark: River Publishers, 2018.
- [3] A. Costanzo et al., "Electromagnetic energy harvesting and wireless power transmission: A unified approach," *Proc. IEEE*, vol. 102, no. 11, pp. 1692–1711, Nov. 2014.
- [4] Cost Action IC1301 Team, "Europe and the future for WPT: European contributions to wireless power transfer technology," *IEEE Microw. Mag.*, vol. 18, no. 4, pp. 56–87, Jun. 2017.
- [5] C. R. Valenta and G. D. Durgin, "Harvesting wireless power: Survey of energy-harvester conversion efficiency in far-field, wireless power transfer systems," *IEEE Microw. Mag.*, vol. 15, no. 4, pp. 108–120, Jun. 2014.
- [6] Z. Popovic, "Cut the cord: Low-power far-field wireless powering," *IEEE Microw. Mag.*, vol. 14, no. 2, pp. 55–62, Mar. 2013.
- [7] E. Falkenstein, D. Costinett, R. Zane, and Z. Popovic, "Far-field RF-powered variable duty cycle wireless sensor platform," *IEEE Trans. Circuits Syst. II, Exp. Briefs*, vol. 58, no. 12, pp. 822–826, Dec. 2011.
- [8] A. Costanzo and D. Masotti, "Energizing 5G: Near- and far-field wireless energy and data trantransfer as an enabling technology for the 5G IoT," *IEEE Microw. Mag.*, vol. 18, no. 3, pp. 125–136, May 2017.
- [9] M. Pinuela, P. D. Mitcheson, and S. Lucyszyn, "Ambient RF energy harvesting in urban and semi-urban environments," *IEEE Trans. Microw. Theory Techn.*, vol. 61, no. 7, pp. 2715–2726, Jul. 2013.
- [10] E. Falkenstein, M. Roberg, and Z. Popovic, "Low-power wireless power delivery," *IEEE Trans. Microw. Theory Techn.*, vol. 60, no. 7, pp. 2277–2286, Jul. 2012.
- [11] T. Furuta, M. Ito, N. Nambo, K. Itoh, K. Noguchi, and J. Ida, "The 500 MHz band low power rectenna for DTV in the Tokyo area," in *Proc. IEEE Wireless Power Transf. Conf. (WPTC)*, May 2016, pp. 1–3.
- [12] V. Palazzi et al., "Design of a ultra-compact low-power rectenna in paper substrate for energy harvesting in the Wi-Fi band," in *Proc. IEEE Wireless Power Transf. Conf. (WPTC)*, May 2016, pp. 1–4.
- [13] T. Ichihara, T. Mitani, and N. Shinohara, "Study on intermittent microwave power transmission to a ZigBee device," in *IEEE MTT-S Int. Microw. Symp. Dig.*, May 2012, pp. 209–212.
- [14] C. Song et al., "A novel six-band dual CP rectenna using improved impedance matching technique for ambient RF energy harvesting," *IEEE Trans. Antennas Propag.*, vol. 64, no. 7, pp. 3160–3171, Jul. 2016.
- [15] R. Scheeler, S. Korhummel, and Z. Popovic, "A dual-frequency ultralow-power efficient 0.5-g rectenna," *IEEE Microw. Mag.*, vol. 15, no. 1, pp. 109–114, Jan./Feb. 2014.
- [16] A. Takacs, H. Aubert, S. Fredon, L. Despoisse, and H. Blondeaux, "Microwave power harvesting for satellite health monitoring," *IEEE Trans. Microw. Theory Techn.*, vol. 62, no. 4, pp. 1090–1098, Apr. 2014.
- [17] J. Estrada, P. Zurek, and Z. Popovic, "Harvesting of aircraft radar altimeter sidelobes for low-power sensors," in *Proc. Int. Appl. Comput. Electromagn. Soc. Symp. (ACES)*, Mar. 2018, pp. 1–2.
- [18] C. Song et al., "A novel quartz clock with integrated wireless energy harvesting and sensing functions," *IEEE Trans. Ind. Electron.*, vol. 66, no. 5, pp. 4042–4053, May 2018.
- [19] H. Lee, J. Tak, and J. Choi, "Wearable antenna integrated into military berets for indoor/outdoor positioning system," *IEEE Antennas Wireless Propag. Lett.*, vol. 16, pp. 1919–1922, 2017.
- [20] S. Gorgutsa, S. Bellemare-Rousseau, P. Guay, A. Miled, and Y. Messaddeq, "Smart T-shirt with wireless respiration sensor," in *Proc. IEEE SENSORS*, Oct. 2017, pp. 1–3.
- [21] M. Wagih, A. S. Weddell, and S. Beeby, "Dispenser printed flexible rectenna for dual-ISM band high-efficiency supercapacitor charging," in *Proc. IEEE Wireless Power Transf. Conf.*, Jun. 2021, pp. 1–4.
- [22] Z. Popović, E. A. Falkenstein, D. Costinett, and R. Zane, "Low-power far-field wireless powering for wireless sensors," *Proc. IEEE*, vol. 101, no. 6, pp. 1397–1409, Jun. 2013.
- [23] A. Dolgov, R. Zane, and Z. Popović, "Power management system for online low power RF energy harvesting optimization," *IEEE Trans. Circuits Syst. I, Reg. Papers*, vol. 57, no. 7, pp. 1802–1811, Jul. 2010.
- [24] Z. Popović et al., "Scalable RF energy harvesting," *IEEE Trans. Microw. Theory Techn.*, vol. 62, no. 4, pp. 1046–1056, Apr. 2014.
- [25] F. Xie, G.-M. Yang, and W. Geyi, "Optimal design of an antenna array for energy harvesting," *IEEE Antennas Wireless Propag. Lett.*, vol. 12, pp. 155–158, 2013.
- [26] S. Shen, C.-Y. Chiu, and R. D. Murch, "Multiport pixel rectenna for ambient RF energy harvesting," *IEEE Trans. Antennas Propag.*, vol. 66, no. 2, pp. 644–656, Feb. 2018.
- [27] F. Erkmen, T. S. Almonneef, and O. M. Ramahi, "Scalable electromagnetic energy harvesting using frequency-selective surfaces," *IEEE Trans. Microw. Theory Techn.*, vol. 66, no. 5, pp. 2433–2441, May 2018.
- [28] W. C. Brown, "An experimental low power density rectenna," in *IEEE MTT-S Int. Microw. Symp. Dig.*, vol. 1, Jul. 1991, pp. 197–200.
- [29] H. Takhedmit, L. Cirio, F. Costa, and O. Picon,

- “Transparent rectenna and rectenna array for RF energy harvesting at 2.45 GHz,” in *Proc. 8th Eur. Conf. Antennas Propag. (EuCAP)*, Apr. 2014, pp. 2970–2972.
- [30] Y. Hu, S. Sun, H. Xu, and H. Sun, “Grid-array rectenna with wide angle coverage for effectively harvesting RF energy of low power density,” *IEEE Trans. Microw. Theory Techn.*, vol. 67, no. 1, pp. 402–413, Jan. 2019.
- [31] K. Nishida et al., “5.8 GHz high sensitivity rectenna array,” in *IEEE MTT-S Int. Microw. Symp. Dig.*, May 2011, pp. 19–22.
- [32] H. Sun and W. Geyi, “A new rectenna using beamwidth-enhanced antenna array for RF power harvesting applications,” *IEEE Antennas Wireless Propag. Lett.*, vol. 16, pp. 1451–1454, 2017.
- [33] E. Kwiatkowski, C. T. Rodenbeck, T. Barton, and Z. Popovic, “Power-combined rectenna array for X-band wireless power transfer,” in *IEEE MTT-S Int. Microw. Symp. Dig.*, Aug. 2020, pp. 992–995.
- [34] H. Sun, Y.-X. Guo, M. He, and Z. Zhong, “A dual-band rectenna using broadband Yagi antenna array for ambient RF power harvesting,” *IEEE Antennas Wireless Propag. Lett.*, vol. 12, pp. 918–921, 2013.
- [35] L. Zhu, J. Zhang, W. Han, L. Xu, and X. Bai, “A novel RF energy harvesting cube based on air dielectric antenna arrays,” *Int. J. RF Microw. Comput.-Aided Eng.*, vol. 29, no. 1, Jan. 2019, Art. no. e21636.
- [36] J. A. Hagerty and Z. B. Popović, “An experimental and theoretical characterization of a broadband arbitrarily-polarized rectenna array,” in *IEEE MTT-S Int. Microw. Symp. Dig.*, vol. 3, May 2001, pp. 1855–1858.
- [37] J. A. Hagerty, F. B. Helmbrecht, W. H. McCalpin, R. Zane, and Z. B. Popovic, “Recycling ambient microwave energy with broad-band rectenna arrays,” *IEEE Trans. Microw. Theory Techn.*, vol. 52, no. 3, pp. 1014–1024, Mar. 2004.
- [38] N. P. Basta, E. A. Falkenstein, and Z. Popovic, “Bow-tie rectenna arrays,” in *Proc. IEEE Wireless Power Transf. Conf. (WPTC)*, May 2015, pp. 1–4.
- [39] J. A. Estrada et al., “RF-harvesting tightly coupled rectenna array tee-shirt with greater than octave bandwidth,” *IEEE Trans. Microw. Theory Techn.*, vol. 68, no. 9, pp. 3908–3919, Sep. 2020.
- [40] H. Mahfoudi, M. Tellache, and H. Takhedmit, “A wideband rectifier array on dual-polarized differential-feed fractal slotted ground antenna for RF energy harvesting,” *Int. J. RF Microw. Comput.-Aided Eng.*, vol. 29, no. 8, Aug. 2019, e21775. [Online]. Available: <https://onlinelibrary.wiley.com/doi/abs/10.1002/mnce.21775>
- [41] U. Olgun, C. C. Chen, and J. L. Volakis, “Investigation of rectenna array configurations for enhanced RF power harvesting,” *IEEE Antennas Wireless Propag. Lett.*, vol. 10, pp. 262–265, 2011.
- [42] S. Shen, Y. Zhang, C.-Y. Chiu, and R. Murch, “An ambient RF energy harvesting system where the number of antenna ports is dependent on frequency,” *IEEE Trans. Microw. Theory Techn.*, vol. 67, no. 9, pp. 3821–3832, Sep. 2019.
- [43] S. Shen, Y. Zhang, C.-Y. Chiu, and R. Murch, “Directional multipoint ambient RF energy-harvesting system for the Internet of Things,” *IEEE Internet Things J.*, vol. 8, no. 7, pp. 5850–5865, Apr. 2021.
- [44] J. A. Hagerty, N. D. Lopez, B. Popovic, and Z. Popovic, “Broadband rectenna arrays for randomly polarized incident waves,” in *Proc. 30th Eur. Microw. Conf.*, Oct. 2000, pp. 1–4.
- [45] J. A. Estrada et al., “An octave bandwidth RF harvesting tee-shirt,” in *Proc. IEEE Wireless Power Transf. Conf. (WPTC)*, London, U.K., Jun. 2019, pp. 232–235.
- [46] H. W. Bode, *Network Analysis and Feedback Amplifier Design*. Van Nostrand, 1945.
- [47] R. M. Fano, “Theoretical limitations on the broadband matching of arbitrary impedances,” *J. Franklin Inst.*, vol. 249, no. 1, pp. 57–83, Jan. 1950.
- [48] A. Kerr, “Some fundamental and practical limits on broadband matching to capacitive devices, and the implications for SIS mixer design,” *IEEE Trans. Microw. Theory Techn.*, vol. 43, no. 1, pp. 2–13, Jan. 1995.
- [49] F. Erez and P. Zoya, “DC power pattern of rectifier-antennas,” in *Proc. 30th URSI Gen. Assem. Scientific Symp.*, Aug. 2011, pp. 1–4.
- [50] E. A. Falkenstein, “Characterization and design of a low-power wireless power delivery system,” Ph.D. dissertation, Dept. Elect., Comput. Energy Eng., Univ. Colorado at Boulder, Boulder, CO, USA, 2012.
- [51] S. Shen, Y. Zhang, C.-Y. Chiu, and R. Murch, “Multiple antennas for wireless power transfer and energy harvesting: Multipoint rectenna design,” *Proc. IEEE*, 2022.
- [52] A. Douyere, F. Alicalapa, J.-D. L. S. Luk, and A. Celeste, “Losses analysis and performance improvement of a rectenna for RFID systems,” in *Proc. 15th IEEE Int. Conf. Electron., Circuits Syst.*, Aug. 2008, pp. 1083–1086.
- [53] H.-K. Chiou and I.-S. Chen, “High-efficiency dual-band on-chip rectenna for 35- and 94-GHz wireless power transmission in 0.13- μm CMOS technology,” *IEEE Trans. Microw. Theory Techn.*, vol. 58, no. 12, pp. 3598–3606, Dec. 2010.
- [54] G. Andia Vera, A. Georgiadis, A. Collado, and S. Via, “Design of a 2.45 GHz rectenna for electromagnetic (EM) energy scavenging,” in *Proc. IEEE Radio Wireless Symp. (RWS)*, Jan. 2010, pp. 61–64.
- [55] Avago. (2007). *Application Note 1124: Linear Models for Diode Surface Mount Packages*. [Online]. Available: https://docs.broadcom.com/wcs-public/products/application-notes/application-note/829/290/av02-0038en-an_1124-21jul10.pdf
- [56] P. S. Hall, J. S. Dachele, and J. R. James, “Design principles of sequentially fed, wide bandwidth, circularly polarized microstrip antennas,” *IEE Proc. H-Microw., Antennas Propag.*, vol. 136, no. 5, pp. 381–389, Oct. 1989.
- [57] B. B. Tierney, C. T. Rodenbeck, M. G. Parent, and A. P. Self, “Scalable, high-sensitivity X-band rectenna array for the demonstration of space-to-earth power beaming,” *IEEE Access*, vol. 9, pp. 27897–27907, 2021.
- [58] *Interpolation*. Accessed: Apr. 1, 2020. [Online]. Available: <https://www.mathworks.com/help/curvefit/interpolation.html>
- [59] C. A. Balanis, *Antenna Theory: Analysis and Design*, 4th ed. Hoboken, NJ, USA: Wiley, 2016.
- [60] D. F. Kelley and W. L. Stutzman, “Array antenna pattern modeling methods that include mutual coupling effects,” *IEEE Trans. Antennas Propag.*, vol. 41, no. 12, pp. 1625–1632, Dec. 1993.
- [61] A. S. Boaventura and N. B. Carvalho, “Maximizing DC power in energy harvesting circuits using multisine excitation,” in *IEEE MTT-S Int. Microw. Symp. Dig.*, Jun. 2011, pp. 1–4.
- [62] D. Belo and N. B. Carvalho, “Harmonic spaced multisines for efficient wireless power transmission,” in *Proc. IEEE Wireless Power Transf. Conf. (WPTC)*, May 2015, pp. 1–4.
- [63] Z. Liu, Z. Zhong, and Y.-X. Guo, “Intermodulation harvesting rectifier design for high efficiency multi-sine wireless power transfer,” in *IEEE MTT-S Int. Microw. Symp. Dig.*, May 2016, pp. 1–3.
- [64] R. Rousseau, G. Villemaud, and F. Hutu, “Efficiency of wireless power transfer with a multi-sine source optimized for the propagation channel,” in *Proc. IEEE Wireless Power Transf. Conf. (WPTC)*, Jun. 2019, pp. 334–337.
- [65] S. Shen and B. Clerckx, “Joint waveform and beamforming optimization for MIMO wireless power transfer,” *IEEE Trans. Commun.*, vol. 69, no. 8, pp. 5441–5455, Aug. 2021.
- [66] A. Collado and A. Georgiadis, “Improving wireless power transmission efficiency using chaotic waveforms,” in *IEEE MTT-S Int. Microw. Symp. Dig.*, Jun. 2012, pp. 1–3.
- [67] A. Collado and A. Georgiadis, “Optimal waveforms for efficient wireless power transmission,” *IEEE Microw. Wireless Compon. Lett.*, vol. 24, no. 5, pp. 354–356, May 2014.
- [68] A. López-Yela, A. López-Yela, D. Segovia-Vargas, and Z. Popovic, “Non-linear diode rectifier analysis for multi-tone wireless power harvesting,” in *Proc. IEEE Int. Conf. Microw., Antennas, Commun. Electron. Syst. (COMCAS)*, Nov. 2019, pp. 1–5.

ABOUT THE AUTHORS

Eric Kwiatkowski (Member, IEEE) received the B.S. degree in electrical engineering from Bucknell University, Lewisburg, PA, USA, in 2015, and the M.S. degree in electrical engineering from the University of Colorado Boulder, Boulder, CO, USA, in 2020.

He was an RF Systems Hardware Engineer with Apple, Cupertino, CA, USA, from 2020 to 2021, an Electromagnetic Design Engineer working on wireless charging applications with Pi Charging, San Bruno, CA, USA, from 2016 to 2018, and a Manufacturing Test Engineer with Lutron Electronics, Coopersburg, PA, USA, from 2015 to 2016. He currently works on active phased arrays at UTVATE, San Francisco, CA, USA. His research was focused on the application of array theory to non-linear rectifying elements for wireless power transfer applications.



José Antonio Estrada (Member, IEEE) received the B.S. degree in electrical engineering from the University of Carabobo, Valencia, Venezuela, in 2012, and the M.S. and Ph.D. degrees in electrical engineering from the University of Colorado Boulder, Boulder, CO, USA, in 2017 and 2021, respectively.

He was an Assistant Lecturer with the University of Carabobo from 2012 to 2015 and a Researcher with the Applied Electromagnetics Laboratory, Fundación Instituto de Ingeniería, Caracas, Venezuela, from 2014 to 2015, working as a Laboratory Coordinator, leading research projects and overseeing electromagnetic compatibility (EMC) compliance and antenna testing. He is currently with the National Institute of Standards and Technology, Boulder. His research interests include the design of cryogenic Josephson-junction-based circuits, quantum measurement, optomechanics, quantum computing, high-efficiency power amplifiers, microwave filters, tuneable RF front ends, front-end miniaturization, heterogeneous integration, energy harvesting, and wireless powering.



Ana López-Yela (Member, IEEE) received the B.S. degree in electrical engineering from the Technical University of Madrid (UPM), Madrid, Spain, in 2013, and the M.S. degree in telecommunications engineering, the M.S. degree in multimedia and communications, and the Ph.D. degree from the University Carlos III of Madrid (UC3M), Madrid, in 2015 and 2020, respectively.



From 2015 to 2016, she worked on the MANA project, for miniaturizing antennas for military aircraft (project in collaboration with the Airbus Defense and Space, Taufkirchen, Germany). She is currently a Microwave Engineer in Madrid, Spain. Her research interests are in electrically small antennas for aircraft communications and in energy harvesting theory and practice.

Dr. López-Yela received a Spanish Ministry of Education, Culture and Sport FPU Fellowship in 2016 for pursuing the Ph.D. degree at UC3M.

Zoya Popović (Fellow, IEEE) received the Dipl.Ing. degree from the University of Belgrade, Belgrade, Serbia, in 1985, and the Ph.D. degree from the California Institute of Technology, Pasadena, CA, USA, in 1990.



She was a Visiting Professor with the Technical University of Munich, Munich, Germany, from 2001 to 2003, and the Institut Supérieur de l'Aéronautique et de l'Espace (ISAE), Toulouse, France, in 2014. She was the Chair of Excellence with the Carlos III University of Madrid, Madrid, Spain, from 2018 to 2019. She is currently a Distinguished Professor and the Lockheed Martin Endowed Chair of Electrical Engineering with the University of Colorado Boulder, Boulder, CO, USA. She has graduated 68 Ph.D.'s and currently advises 18 doctoral students. Her current research interests include high-efficiency power amplifiers and transmitters, microwave and millimeter-wave high-performance circuits for communications and radar, medical and industrial applications of microwaves, wireless powering, and quantum sensors.

Dr. Popović was elected as a Foreign Member of the Serbian Academy of Sciences and Arts in 2006. She was a recipient of two IEEE MTT-S Microwave Prizes for best journal papers, the White House NSF Presidential Faculty Fellow Award, the URSI Issac Koga Gold Medal, the ASEE/HP Terman Medal, and the German Humboldt Research Award. She was named the IEEE MTT Distinguished Educator in 2013 and the University of Colorado Distinguished Research Lecturer in 2015.